Preprint
UCRL-JC-148789

High Intensity Beam and X-Ray Converter Target Interactions and Mitigation

Y.-J. Chen, J.F. McCarrick, G. Guethlein, F. Chambers, S. Falabella, E. Lauer, R. Richardson, J. Weir

This article was submitted to
10th Advanced Accelerator Concepts Workshop, Oxnard, California, June 23-28, 2002

July 31, 2002

U.S. Department of Energy
Lawrence Livermore National Laboratory

High Intensity Beam and X-Ray Converter Target Interactions and Mitigation

Yu-Jiuan Chen, James F. McCarrick, Gary Guethlein, Frank Chambers, Steven Falabella, Eugene Lauer, Roger Richardson, and John Weir

Lawrence Livermore National Laboratory, PO Box 808, L-645, Livermore, CA 94550, USA

Abstract. Ions extracted from a solid surface or plasma by impact of an high intensity and high current electron beam can partially neutralize the beam space charge and change the focusing system. We have investigated ion emission computationally and experimentally. By matching PIC simulation results with available experimental data, our finding suggests that if a mix of ion species is available at the emitting surface, protons dominate the backstreaming ion effects, and that, unless there is surface flashover, ion emission is source limited. We have also investigated mitigation, such as e-beam cleaning, laser cleaning and ion trapping with a foil barrier. The temporal behavior of beam spot size with a foil barrier and a focusing scheme to improve foil barrier performance are discussed.

1 INTRODUCTION

The second axis of the Dual Axis Radiographic Hydrodynamic Test facility (DARHT-II) [1, 2] will deliver multiple electron pulses to a converter target to produce x-ray pulses (with spot sizes ≤ 2.1 mm) for flash radiography. Performance of high resolution x-ray radiography facilities requires high current electron beams to be focused to a millimeter spot size on an x-ray converter throughout the entire current pulse. Several effects, such as target plasma created by preceding pulses, and the backstreaming ion effect [3], may impact the spot size. We have designed the DARHT-II x-ray converter target to minimize expansion of target plasma into the incoming beam's path [4, 5, 6]. Thus, the spot size changes from pulse to pulse due to the charge neutralization effects of the target plasma are small. However, the time varying focusing forces of backstreaming ions pulled from the desorbed gas at the target surface or from a pre-existing target plasma plume by the electron beam's strong electric field could potentially and drastically change the spot size.

We have investigated backstreaming ion emission and mitigation both computationally and experimentally. In Sec. 2, we show that comparison between PIC simulation results and the available experimental data indicates that if a mix of species is available, protons dominate the backstreaming ion effect, and that ion emission may be source limited. Section 3 shows that we have demonstrated experimentally that backstreaming ion effects can be minimized by pre-cleaning target surfaces with an electron beam or a laser. Hughes first suggested the use of a foil to confine backstreaming ions within a short distance so that the focusing effect is tolerable [7].

We have investigated the foil-barrier scheme experimentally and computationally as well; the results will be discussed in Sec. 4. We will discuss how the tuning strategy for beam transport affects the foil-barrier scheme's performance and how the backstreaming ions with mitigation affect the on-axis x-ray dose in Sec. 5. A summary is presented in Sec. 6.

2 ION EMISSION FROM FOILS

It is a concern that ions desorbed from solid surfaces by an incoming DARHT-II beam (18.6 MeV, 2 kA and 2μs) and subsequently accelerated and trapped by the beam space charge potential will provide unwanted charge neutralization to the beam, upsetting the transport system. These ion focusing effects were studied on the 19.8-MeV, 2-kA DARHT double foil experiment [8]. The beam was focused onto a thin foil to minimize the beam scattering. The ions generated by the beam moved both upstream and downstream to form ion channels on the both sides of the foil. The ion focusing effects were then observed by measuring the time-varying beam radius on a downstream witness foil. A similar experiment [9], which had similar sensitivities and operated at similar energy densities on some of the same types of materials, was performed at the 6-MeV, 2-kA ETA-II facility. Comparing PIC simulation results with data available from these two experiments provides us some understanding of ion emission.

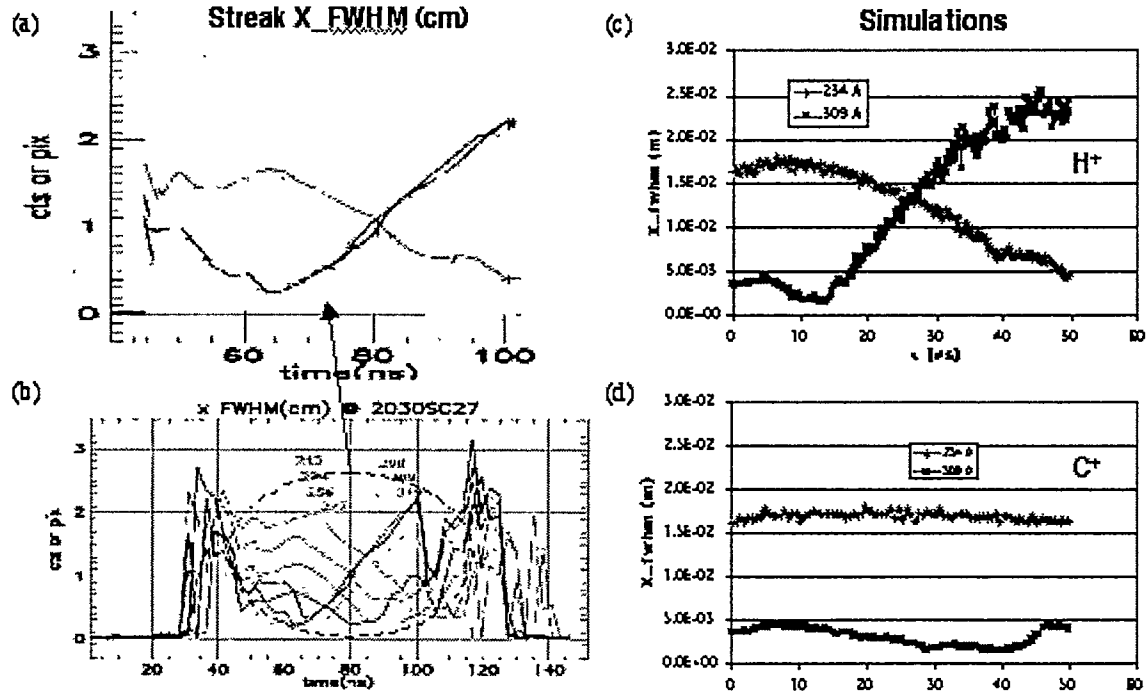

FIGURE 1. The ETA-II temporal beam radius profiles on the witness foil when flashover occurred on the quartz foil. The curves in (a) are taken from the data shown in (b) (adopted from Ref. [9]). Two curves in (a) the experimental data, (c) simulations with space-charge-limited emission for protons and (d) simulations with space-charge-limited emission for C+ are for two magnet settings.

The potential species for an ion channel are protons and oxygen from the water vapor on the foil surface, carbon, and the foil material itself. The lighter ions have a greater potential to destroy electron beam's final focus since they would travel upstream and downstream at a higher speed and form a longer ion channel. The ions from the foil material itself are usually too heavy to have a large effect on the beam spot size during the beam pulse time. One foil material used on the ETA-II double foil experiment for ion emission was quartz. The ETA-II beam impinging on the dielectric surface created flashover and a rich ion source for space charge limited emission at t = 0. Shown in Fig. 1 are the temporal profiles of the beam radius on the witness foil obtained from PIC simulations, in which space charge limited protons are emitted from t = 0, and the experimentally measured profiles. The match is quite good and is obtained without any additional fitting parameters. The simulated profiles do not match the data when other heavier ions are used in the simulations (see Fig.1d). These comparisons suggest that if a mix of species is available, protons may dominate the backstreaming ion effects; however, simulations where multiple species are available have not been done, as this requires more sophisticated modeling of the emission sheath. Given the quality of the match and lacking any direct measurements of the emitted species, all the simulations presented later in this paper assume only protons emitted from a surface.

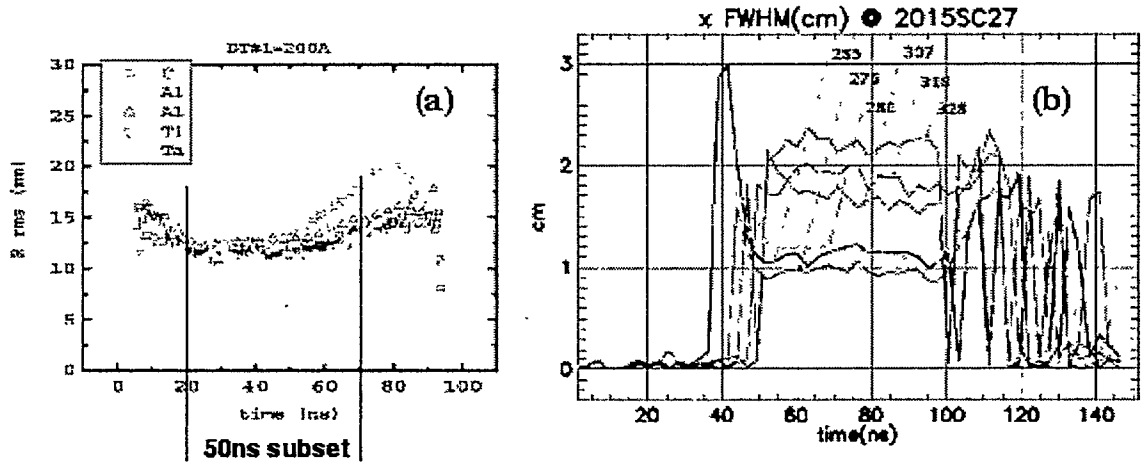

FIGURE 2. Beam spot behaviors from (a) DARHT-I (adapted from Ref. [8]), and (b) ETA-II (adopted from Ref. [9]) double foil experiments.

Typical results from both the DARHT and ETA-II double foil experiments are shown in Figs. 2a and b. The DARHT data show that there is a source of ions even at relatively low temperatures [8]. However, the ETA-II data did not show any ion emission effects [9] even though the experiments had similar sensitivities and energy densities on some materials. Since the different beam energies for these two experiments does not play a significant role in any proposed ion production mechanism, the two remaining differences are that ETA-II has a shorter current flattop (50 ns rather than 70 ns), and that the materials which showed the strongest effect on DARHT-I (Ta and Ti) were not used on ETA-II. In order to reconcile the results, an

ion emission model somewhat more detailed than simple space charge limited (SCL) emission is required.

PIC simulations assuming SCL conditions for various species do not match either experiment. The resulting beam disruption would occur much sooner and be much stronger than what is observed on DARHT-I. Models used in [8] which delay the onset of SCL emission until the barrier material reaches a threshold temperature can match the onset time but not the rate of beam disruption. A model that has two knobs, one for the onset time and one for the slope, must be considered. Such a model was proposed in [10] and has been used in this paper for PIC simulations of both the ETA-II and DARHT-I experiments. A quick summary of the model is a follows:

The desorption of neutral gas from the foil surface is determined by a simple rate equation that is a strong function of temperature. The areal density of neutrals is given by

$$\frac{dN}{dt} = \nu(N_s - N)e^{-E_b/T} \qquad (1)$$

where N is the number of desorbed neutrals per unit area, N_s is the initial density of adsorbates on the surface, ν is a rate coefficient, and E_b is an energy that characterizes the nature of the adsorption. The initial adsorbate density, N_s, is measurable and is of the order 10^{15} cm^{-2}. The rate coefficient , ν, is roughly of order 10^{13} s^{-1}, but is a much less sensitive parameter than E_b, which is basically a fitting parameter that controls the onset time of the beam disruption in the experiment. The exponential temperature dependence results in behavior characterized by a threshold temperature at which all of the adsorbed gas is released. Sample curves for a linear heating rate are shown in Fig. 3.

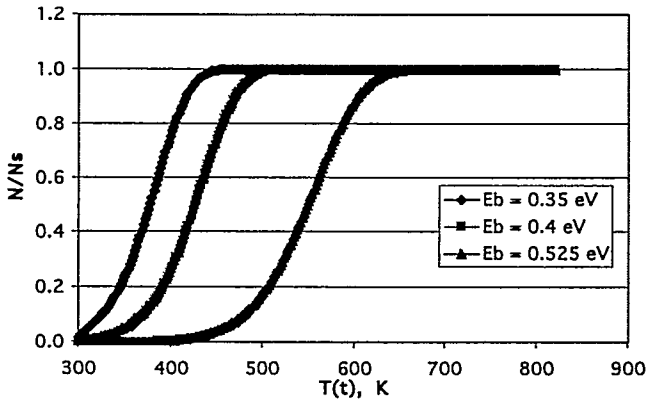

FIGURE 3. Gas desorption model given linear temperature rise, for various binding energies.

The next ingredient is an ionization model. The two extremes are to assume that avalanche breakdown occurs immediately in the desorbed species, a quite strong effect, or that only beam impact ionization occurs, which is weak at these electron energies. The former assumption quickly enters the SCL regime, since only a small fraction of a monolayer of ions is needed to reach the space charge limit. The latter assumption is also modeled with a simple rate equation

$$\frac{dN_i}{dt} = \frac{\sigma N J_b}{q} \qquad (2)$$

where N_i is the areal ion density, σ is the impact ionization cross section, J_b is the beam current density, and q is the unit charge. The ion emission current is then bound by the smaller of the SCL value or the quantity $\sigma N J_b$. The ionization cross section in the energy range of 6 – 20 MeV is of order 2.5×10^{-19} cm^2. The solution of Eqs. (1) and (2) is proportional to the product of σ and the areal adsorbate density, which includes the number of monolayers on the surface and is not exactly known. Thus the product σN_s is a second fitting parameter for the experimental data, yielding the slope of the beam disruption.

Consider a subset of the DARHT-I data consisting of the first 50 ns of the flattop and compare it to the flattop data from ETA-II (see Fig. 2). Since the curves for Ta and Ti are not available for ETA-II, it becomes clear that 50 ns is not long enough to resolve the ion effect above the error bars of the ETA-II data. Thus the experimental data can be matched by adjusting E_b to produce an onset later than would be resolved on ETA-II, and then adjusting σN_s to produce the correct slope of the DARHT-I data thereafter. Figure 4 shows the results of a simulation assuming a binding energy of 0.47 eV and 3 monolayers of adsorbed gas, using the nominal cross section given above, compared with the 70 ns flattop of the DARHT data (with the Ta and Ti curves removed).

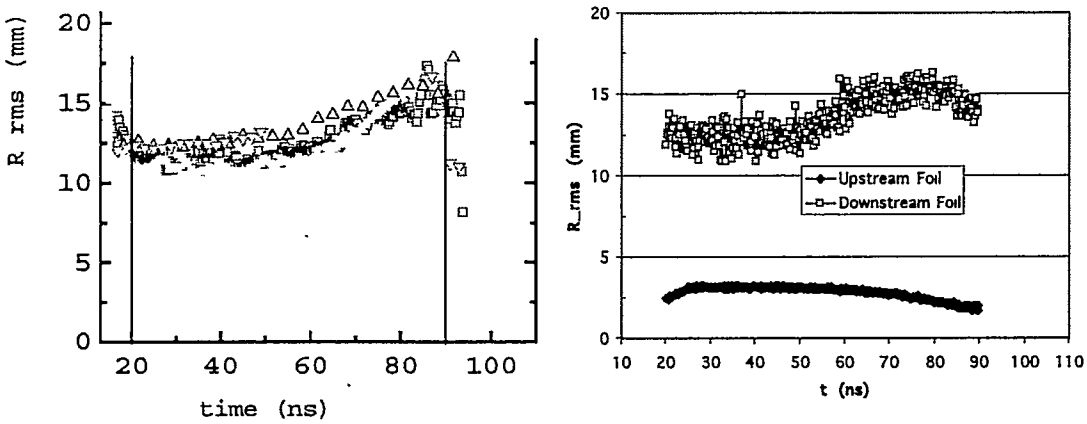

FIGURE 4. Comparison of 70 ns DARHT-I flattop data (left) with simulated gas desorption/ionization model (right).

As mentioned earlier, the simulations presented here only involve one species of ions, namely protons; however, it is unlikely that simulations with multiple SCL species can match simultaneously the rapid beam disruption shown in Fig. 1 and the slow disruption shown in Fig. 2. Although the simple model given by Eqs. 1 and 2 glosses over the mix of physics giving rise to gas desorption, it does serve to reconcile the available experimental data and gives a rough quantification of emission current, showing that it is source limited. It is possible that surface cleaning will be sufficient to avoid this type of emission from the barrier surface.

3 SURFACE CLEANING

As discussed in the previous section, without a pre-existing plasma created on the target surface, the spot disruption on the 6–MeV, 2-KA ETA-II beam due to the backstreaming ions was weak during its flattop. To simulate the DARHT-II beam-target interactions, backstreaming ion emission and surface cleaning were studied on the ETA-II/SNOWTRON double pulse facility [11]. First, plasma was created by striking the 1-MeV, 2-kA Snowtron beam on one side of a foil. The better characterized ETA-II beam entered from the other side to probe the beam-target interactions. Typically five diagnostics were taken for each shot. Backstreaming ions were collected by a Faraday cup at the ETA-II side. On-axis x-ray dose generated by the ETA-II beam was measured through a pair of apertures along a path that included the SNOWTRON cathode. The ETA-II x-ray spots at 10 ns before and 15 ns after the center of the flattop were recorded by imaging the optical transition radiation from the target. The time integrated SNOWTRON beam spot was taken by an optical framing camera.

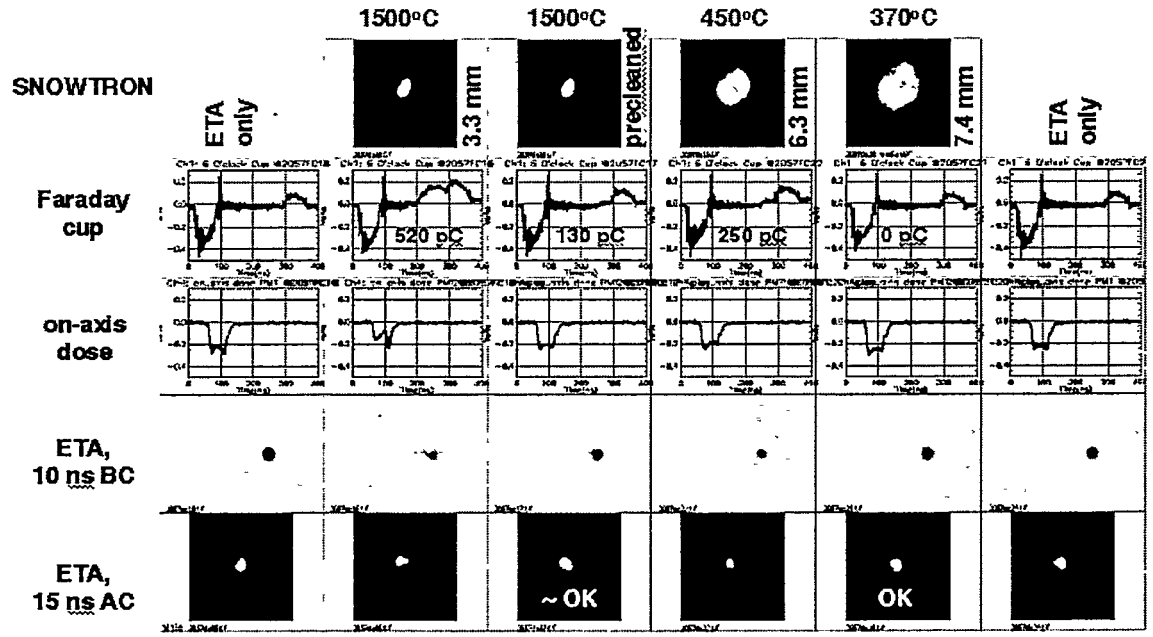

FIGURE 5. Faraday cup's ion signals, beam spot sizes and x-ray forward doses for the electron beam cleaning experiment

Figure 5 presents a set of results for e-beam cleaning of a 3-mil graphite foil. The first and the last columns present the nominal data when the SNOWTRON beam was not fired and no plasma created. Note that no ion signals were detected by the Faraday cup for the nominal cases. Columns 2-4 present data for various SNOWTRON spot sizes. The calculated peak foil temperature based on energy deposition is given on the top of each column. The separation between the SNOWTRON beam and the ETA-II beam was 2 μs for this set of data. The total ion charge collected by Faraday cup is

also shown with each Faraday cup data. The SNOWTRON beam spot sizes for Columns 2 and 3 were the same. However, for the pre-cleaned case, SNOWTRON was fired twice with a 1-second separation. The Faraday cup signal indicates that the first pulse cleaned the foil surface and reduced ion emission. The data also show that e-beam cleaning preserved the beam spot size and on-axis x-ray dose. Comparing Columns 4 and 5 suggests that ion emission due to gas desorption occurs around 400°C, which agrees with observations on ion emission in an IVA diode reported in Ref. [12].

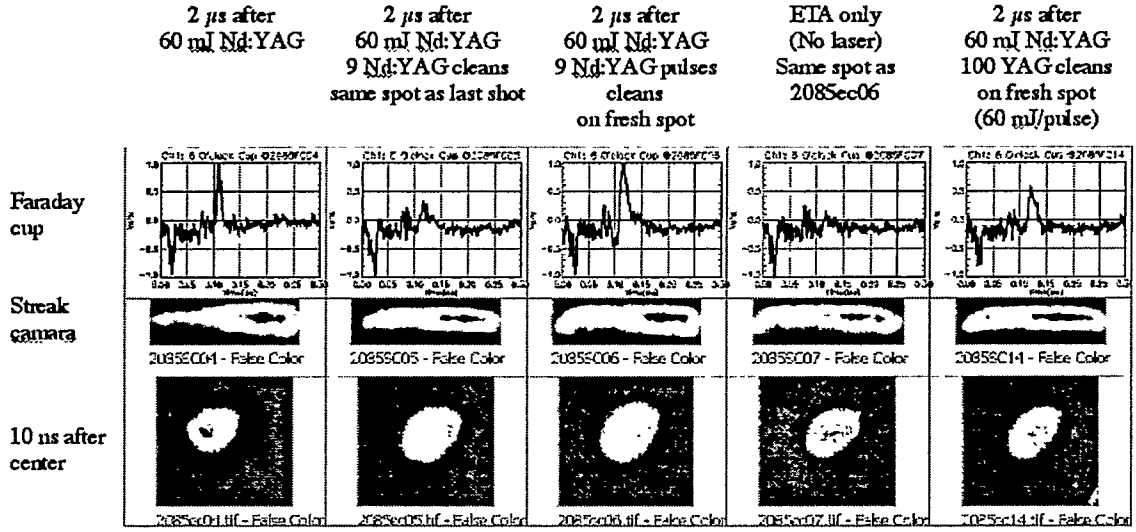

FIGURE 6. The ETA-II beam spot sizes corresponding to the number of pre-cleaning laser pulses.

We have also investigated using a pulsed laser to pre-clean graphite foil. A 6-mil graphite foil, which was backed with a 10-mil quartz foil serving as a Cherenkov witness foil, was used as a target. A 60-mJ Nd:YAG laser at 1.06 μm was used to pre-clean the graphite. Since the backstreaming ions' spot size disruption effects on the ETA-II beam is weak without a pre-existing plasma, the laser was also used to create plasma on the graphite foil surface at 2 μs before the ETA-II beam was fired. Without pre-cleaning, the beam blew up rapidly in the presence of ions and formed a large halo (see the first column in Fig. 6). The image of the halo is barely visible because that the x-ray intensity created by the halo was small. The laser spot used for pre-cleaning and e-beam disruption was about 5 mm in diameter. We found that the ETA-II spot was preserved if the separation between the last laser cleaning pulse and the ETA-II beam is around 1 second. Figure 6 shows that firing 9 or more laser pulses on a foil with a prior cleaning history, or 100 pulses on a foil with no prior cleaning history, can effectively preserve the beam spot size through the entire beam flattop. Presumably those laser pulses have cleaned the graphite surface. Note that the data presented in the "ETA only" column was taken when the ETA-II beam was impinging on an old spot used by the shot corresponding to the data in the 3rd column. The surface had been cleaned by both the 9 laser cleaning pulses and the e-beam, and hence, the data represents the best possible beam spot behavior for the ETA-II beam.

4 FOIL BARRIER AND IONS' TRANSIENT BEHAVIOR

Mitigation of backstreaming ion effects with a foil-barrier was demonstrated on the ETA-II/SNOWTRON double pulses facility [13]. When plasma is created by the SNOWTRON beam 600 ns prior to the ETA pulse, the focus of the ETA-II beam was destroyed within 20 ns if a foil-barrier was not used. However, if a grounded foil was placed 1 cm in front of the ETA-II side of the target, the spot size was preserved through the entire ETA-II flattop.

While the use of a grounded foil to stop backstreaming ions has been successful, some time-dependent focusing remains. Consider that the ions are emitted from the grounded target surface and are impeded by the grounded foil barrier. Since the transverse electric field of the beam is sufficiently large to cause surface flashover and to lead to unpredictable or at least unreliable behavior, both surfaces are grounded as a requirement. The region between the two ground planes has a strong potential well due to the beam space charge. If the geometry were one dimensional – a slab of charge between two sheets – it is clear that the region would act, under ideal circumstances, as a trap for the ions, and that the target and the barrier foil act as turning points for ions born at zero energy. What is not as obvious is that, due to the two dimensional nature of the system and, to a lesser extent, time dependence of the beam current, the trapping effect is "robust", and that ideal conditions such as zero emission energy are not necessary. The result is that ion charge accumulates between the target and barrier, and moves towards a steady-state configuration of complete neutralization of the electron beam. The stability of such an equilibrium and the existence of a physical path towards it are not addressed in this paper. What is important is that at the start of a beam pulse, there are no ions (i.e., a neutralization fraction, f, of 0) and that the system evolves with time towards $f = 1$. The spatial profile of the neutralization evolves as well. The effect of this dynamic evolution on the beam focus (and resulting X-ray spot size) is the concern.

PIC simulations of a baseline DARHT-II target/barrier system have been performed to study the evolution of the system. The simulation transports a K-V electron beam from the downstream side of the foil barrier to the target. The phase space is chosen to produce a 1 mm edge radius beam at a waist on the target surface, at a full current of 2 kA, an energy of 18.4 MeV, and an un-normalized edge emittance of 4 cm-mrad, when no ions are present. The beam current is given a 5 ns rise time from zero at the start of the simulation (t = 0), so that the beam radius is somewhat smaller initially (about 0.8 mm) than at the full-current value. The target is assumed to emit backstreaming ions under space charge limited conditions, from an area corresponding to the nominal beam focus. Self-consistent space charge and current effects are included. Since only the trap region from the foil barrier to the target is simulated, emittance growth due to scattering by the foil barrier and the upstream portion of the barrier foil-focusing are not included in the simulations. The foil barrier and the target are 4 cm apart and the beam pipe (also at ground) is 5 cm in radius.

Figure 7 shows the evolution of the beam size on the target, as an r. m. s. value in the X transverse plane, and the ion current density averaged over the emitting surface.

For a uniform beam, the edge radius would be twice the x_{rms} size. We consider the curves labeled "No bias" first; the other curves will be discussed later. The beam size (Fig. 7a) is characterized by a period of fast initial growth followed by smaller (±10%) variations about a rough value of 0.5 mm. The initial growth corresponds to an early spike in the ion emission current (Fig. 7b) as the beam current rises to its flattop value, producing a "belch" of ions that over focus the electron beam. The subsequent variations are characteristic of electron beam/backstreaming ion behavior. As the beam is over focused and the size on the target grows, the space charge limited ion current drops. The beam experiences less over focusing, and the spot size shrinks, which leads to increase in the axial electric field, and therefore the ion current, and so forth. The initial current spike in the graph diminishes the fact that, at later times, the ion current is experiencing roughly 50% variation, between 2 and 3 MA/m^2. The very gradual decaying ion current curve shows that the effective "fill time" of the trap is much longer than the beam pulse. Figure 8 shows four snapshots of the ion $z/\gamma\beta_z$ phase space, taken at 5, 25, 50, and 80 ns, which also show the slow filling of the trap.

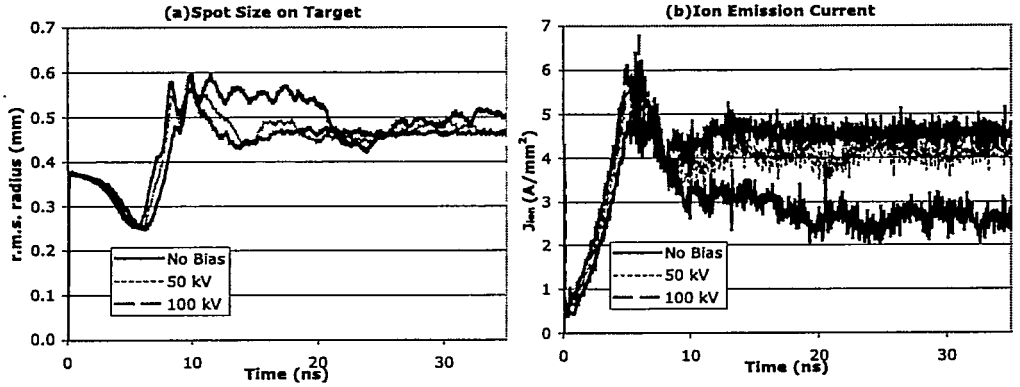

FIGURE 7. Temporal behaviors of (a) beam spot size on the target, as r. m. s. value in the X plane, and (b) ion emission current averaged over the emitting surface. The nominal x_{rms} for the beam without ions is 0.5 mm.

The robust nature of the trap stems from the radial degrees of freedom for the ions. An axial turning point does not correspond to zero ion velocity, but rather pure radial motion. As ions decelerate near the foil barrier, the accumulation of positive charge (which exceeds the beam density at the barrier, although to a lesser extent than at the effective A-K gap near the target) deflects subsequent ions radially, so that v_z can be zero even though the potential is not zero. Also, during the ion "belch" phase, the potential well is deepening as the beam current rises. Therefore, even before any reflection has taken place, the ions are not all experiencing the same accelerating conditions.

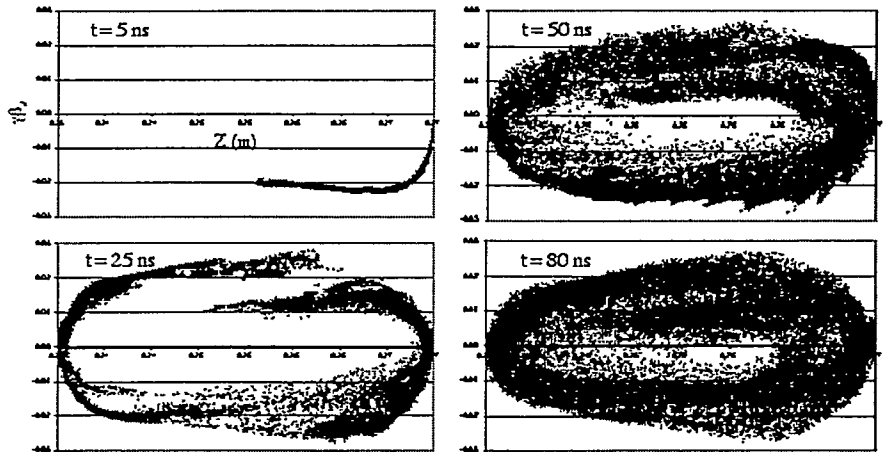

FIGURE 8. Snapshots of the z-$\gamma\beta_z$ ion phase space in the nominal case.

The long fill time of the trap and the transient behavior may not lend themselves to a "clean" performance of the target system from a radiographic standpoint. As shown in Fig. 7a, while the foil barrier scheme does minimize beam disruption reasonably well, the time integrated spot size is better preserved by the foil barrier scheme for a long pulse beam than for a short pulse beam. A possible route around such behavior is to open the trap. Under ideal circumstances one would use a dielectric rather than a conducting foil barrier, but this idea fails in practice due to surface flashover, as mentioned earlier [9]. Another possibility is to employ a bias voltage so that the ions are not emitted at zero energy. Bias schemes have been investigated in the past [14, 15], where the bias voltage is used to trap the ions. In the present case, however, the bias voltage is of opposite polarity to intentionally drive the target/barrier system like an ion diode. How to maintain such a bias on a target being struck by a high-intensity electron beam is not clear. However, one can gloss over such difficulties in a simulation to see if the idea has merit. The answer is that it does not, in fact, solve all the problems.

PIC simulations have been performed using a geometry and beam conditions similar to those above, but now the target is assumed to not fill the beam pipe. It is a conducting disk a few beam radii in size, held at positive voltage with respect to the beam pipe and the foil barrier. The foil barrier is assumed to be a perfect absorber of ions that reach it. Runs have been done at bias voltages of 50 and 100 kV. The ion emission current and resulting beam spot sizes are the additional curves shown in Fig. 8. The ions now have sufficient energy so that they all strike the barrier; thus the system does settle into a rough steady-state with nearly fixed emission current. However, the initial beam spot transient is not eliminated and some of the oscillatory behavior as the beam over- and re-focuses on the target remains. At 100 kV, most of the latter is eliminated. However, it is not clear that this is a sufficient benefit to counter the implementation difficulties of the bias voltage.

5 FOIL-BARRIER AND FOCUSING SCHEME

Performance of the foil-barrier scheme for spot size preservation requires minimizing the backstreaming ions' focusing effects to a tolerable level. The scaling law for the ion channel's disruption length L_D [16] is given as $L_D \cong (\pi\gamma\beta^2 I_o/fI)^{1/2}a$, where I and I_o is the beam current and Alfven current, respectively, f is the ion neutralization fraction, and a is the beam radius. This scaling law indicates that the suitable foil-target separation depends on the overall beam envelope inside the ion trap region, and that the final spot size is sensitive to the beam radius and ions' neutralization fraction. For a single pulse machine, the foil can be placed closely to the target to minimize the spot size sensitivity. However, the spot size on a closely placed foil will be too small to be practical for a multi-pulse machine since the foil may not survive the impact of multiple beam pulses. Instead of shortening the foil-target separation, the foil-barrier's performance can also be improved without sacrificing the final spot size and the x-ray dose by using a different focusing scheme to obtain a larger beam envelope in the ion trap region. This results in weaker ion focusing forces and a larger beam spot on the foil, which is preferable for foil survivability.

We have investigated computationally several tuning schemes with various foil locations to achieve a larger spot size on the foil barrier without sacrificing the nominal spot size on the target. The DARHT-II target configuration is used again. For the results presented in this section, the nominal focal length is 32 cm. The DARHT-II beam near the x-ray converter is 18.4 MeV, 2 kA with a 1-mm radius (0.7-mm r.m.s.). The particle simulations, mentioned in the previous section, indicate that the charge neutralization fraction of those trapped ions near the end of DARHT-II 4th pulse is a function of the distance normalized to the foil-target separation (z/L). To allow a fast parameter study of various focusing schemes, an envelope equation is solved by using a fit for the simulated charge neutralization fraction. Foil focusing effects and lens' aberrations are not modeled by the envelope equation. The spherical aberration and chromatic aberration of the solenoid lens are irrelevant to this section's discussion. The foil focusing effects are insignificant due to the small beam size near the foil. Our particle simulations indicate that the spot size changes due to the foil focusing effects are only a few percent.

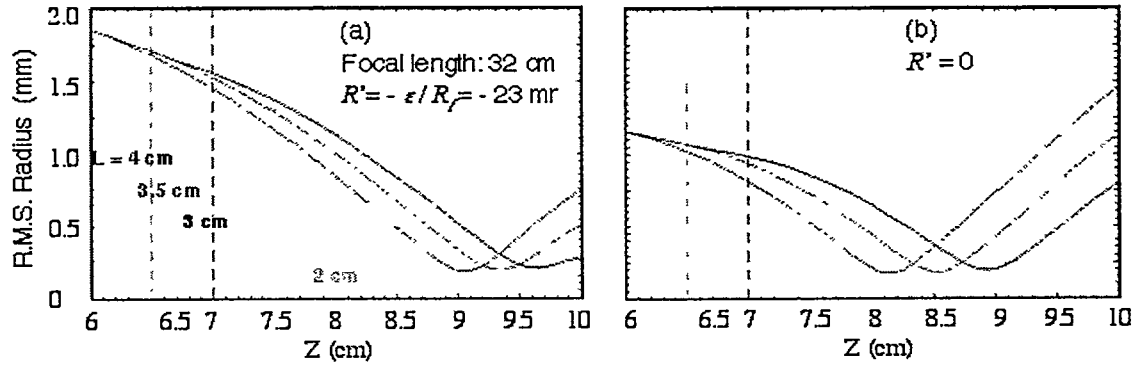

FIGURE 9. The r. m. s. beam envelopes in the foil-barrier traps with various foil-target separations

Figure 9 shows the r. m. s. beam envelopes (curves) with a foil (vertical dashes) placed at 4, 3.5, 3, 2.5, 2 or 0 cm in front of the target surface. The beam is focused beyond the target front surface in Fig. 9a and on the front surface in Fig. 9b. The focusing scheme used for Fig. 9a is better for a multi-pulse machine since the foil can be placed further upstream from the target, and hence, the beam size on the foil is larger for better foil survivability. Comparison between the envelope curve corresponding to a 4-cm separation in Fig. 9a and that corresponding to a 3-cm separation in Fig. 9b suggests that, when the final beam spot size is similar after beam traveling through the ion trap, the resulting beam divergence is also similar. Therefore, the forward x-ray doses created by beams with the same spot sizes but using different focusing schemes and target-foil separations should be similar. The beam divergence at the x-ray converter corresponding to the envelopes in Fig. 9a is shown as a function of the foil-target separation in Fig. 10. The envelope slope (R'), thermal spread (θ_{th}) and the effective divergence are plotted. Since the effective divergence for various foil-target separations remains small compared with the scattering angle accumulated in a 1-mm Ta, the effects of a convergent beam hitting the x-ray converter on the forward x-ray dose should not be an issue.

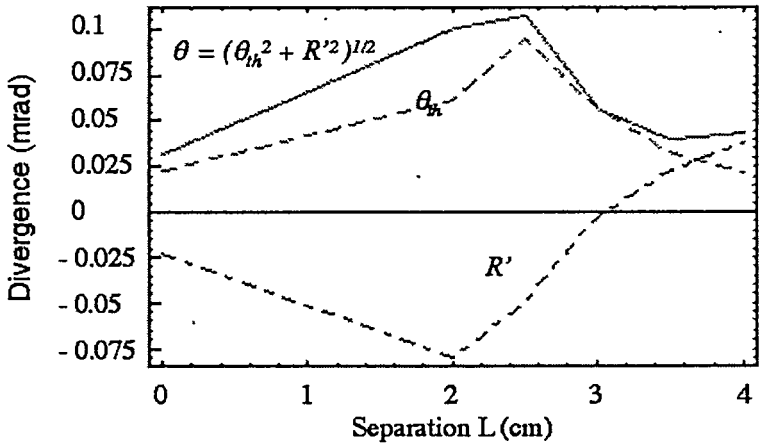

FIGURE 10. The beam divergence at the x-ray converter when an underfocusing scheme is used.

4 SUMMARY

It is a concern that ions desorbed from solid surfaces by an incoming electron beam, and subsequently accelerated and trapped by the beam space charge potential, will provide unwanted charge neutralization to the beam, upsetting the transport system. We have investigated these ions' focusing effects computationally and experimentally. Our finding suggests that if a mix of ion species is available at the emitting surface, protons dominate the backstreaming ion effects, and that, unless there is surface flashover or other pre-existing plasma, ion emission is source limited. While the mechanisms of ion emission from either a solid surface or plasma are still not understood, ion emission can be minimized by cleaning the surface with an electron

beam or several laser pulses. The unwanted ion focusing effects can also be minimized by using a grounded foil to trap ions in a small region. However, the beam radius will exhibit some transient behavior due to the trapped ions' long fill time in the longitudinal phase space. Finally, the foil-barrier's performance in terms of spot size sensitivity to beam parameters and foil survivability can be improved by using a focusing scheme which provides a large beam envelope with a fast convergence in the trap region.

ACKNOWLEDGMENTS

The authors would like to thank G. Caporaso and S. Sampayan for valuable discussions. This work was performed under the auspices of the U.S. Department of Energy by University of California Lawrence Livermore National Laboratory under contract No. W-7405-Eng-48.

REFERENCES

1. M. J. Burns, et al., "Status of the DARHT Phase 2 Long-Pulse Accelerator", *Proceedings of the 2001 Particle Accelerator Conference*, Chicago, Illinois, 2001, pp. 325-329.
2. M. J. Burns, et al., "Status of the Dual Axis Radiographic Hydrodynamics Test (DARHT) Facility", *Proceedings of the 14th High-Power Particle Beams,* Albuquerque, New Mexico, 2002.
3. D. R. Welch and T. P. Hughes, Laser Part. Beams **16**, 285-294 (1998).
4. P. A. Pincosy, et al., "Multiple pulse electron beam converter design for high power radiography", *Review of Scientific Instruments*, **72**, 2599-2604 (2001).
5. D. D.-M. Ho, et al., "Hydrodynamic Modeling of a Multi-Pulse X-Ray Converter Target for DARHT-II", LLNL Report No. UCRL-JC-1442, July 26, 2001.
6. Y.-J. Chen, et al., "Downstream System for the Second Axis of the DARHT Facility", *Proceedings of the XXI LINAC,* Gyeongju, Korea, Aug. 19-23, 2002.
7. T. P. Hughes, "Target Calculations for ITS Short-Focus Experiment", MRC/ABQ-N-589, September 1997.
8. H. A. Davis, et al., "Electron Beam Disrupiton due to Ion Release from Targets – Experimental Observations." *Proceedings of the 14th International Conference on High-Power Particle Beams*, Albuquerque, New Mexico, 2002.
9. E. L. Lauer, et al., "Characterization of the Backstreaming Ion Defocusing Effect Using A Double Foil Measurement Technique." *Proceedings of the 14th International Conference on High-Power Particle Beams,* Albuquerque, New Mexico, 2002.
10. B. V. Oliver, et al., "Beam-Target Interactions in Single- and Multi-Pulse Radiography." Report MRC/ABQ-R-1909, Mission Research Corporation, Albuquerque, New Mexico, 1999.
11. Y.-J. Chen, et. al., "Physics Design of the ETA-II/Snowtron Double Pulse Target Experiment", *XX International LINAC Conference*, Monterey, California, 2000, pp. 482-484.
12. Sanford, T. W. L., et al., *J. appl. Phys.* **66**, 10-22 (1989).
13. S. Sampayan, et. al., "Beam-Target Interaction Experiments for Multipulse Bremsstrahlung Converters Applications", *Proceedings of the 2001 Particle Accelerator Conference*, Chicago, Illinois, 2001, pp. 330-332.
14. T. Kwan, et al., "Design Simulation for Spot Size Stabilization in ITS/DARHT." *Proceedings of the 19th International Linear Accelerator Conference*, Chicago, IL, 1998, pp. 660-662.
15. J. McCarrick, T. Houck. "The Effect of Trapped Backstreaming Ions on Beam Focus and Emittance in Radiographic Accelerators." *Proceedings of the 1999 Particle Accelerator Conference*, New York, New York, 1999, pp. 2755-2757.
16. Caporaso, G. J. and Chen, Y.-J., *Proc. of the XIX LINAC Conference*, Chicago, Illinois, 1998, pp. 831-833.